Nanoscale

ROYAL SOCIETY OF CHEMISTRY

COMMUNICATION

View Article Online
View Journal | View Issue

Cite this: *Nanoscale*, 2021, **13**, 17737

Received 21st September 2021,
Accepted 29th September 2021

DOI: 10.1039/d1nr06214j

rsc.li/nanoscale

Mitochondria targeted composite enzyme nanogels for synergistic starvation and photodynamic therapy†

Zheng Luo,‡[a] Xiaotong Fan,‡[b] Ying Chen,[a] Xiyu Lai,[a] Zibiao Li, *[b,c] Yun-Long Wu *[a] and Chaobin He *[b,c]

Mitochondria, as the energy factory of cells, often maintain a high redox state, and play an important role in cell growth, development and apoptosis. Therefore, the destruction of mitochondrial redox homeostasis has now become an important direction for cancer treatment. Here, we design a mitochondrial targeting composite enzyme nanogel bioreactor with a circulating supply of O_2 and H_2O_2, which is composed of mitochondrial target triphenylphosphine (TPP), natural enzymes glucose oxidase (GOX) and catalase (CAT), and protoporphyrin IX (PpIX). The nanogel can effectively increase the stability of the natural enzymes, and its size of about 65 nm makes them close in space, which greatly improves their cascade catalytic efficiency and safety. Under the action of target TPP, the system can accurately target the mitochondria of breast cancer 4T1 cells, catalyze intracellular glucose to generate H_2O_2 through GOX, and H_2O_2 is further used as a catalytic substrate for CAT to generate O_2. This O_2 can not only further improve the catalytic efficiency of GOX, but also provide raw materials for the production of ROS in PDT, which can effectively destroy the mitochondria of cancer cells, thereby causing tumor cell apoptosis. Compared with GOX alone, thanks to the close spatial position of the composite enzymes, the composite enzyme nanogel can quickly consume the highly oxidative H_2O_2 produced by GOX, thereby showing better safety to normal cells. In addition, the composite enzyme group under light showed excellent antitumor effects by combining starvation therapy and PDT under adequate oxygen supply in animal experiments. In general, this composite enzyme nanogel system with good stability, high safety and excellent cascade catalytic efficiency opens a new way for the development of safe and efficient cancer therapeutics.

Mitochondria are important bioenergy power plants, biosynthesis factories and bioinformation centers of cells, which play an important role in cell differentiation, information transmission and apoptosis. These multifaceted functions make them important cell pressure sensors and enable cells to adapt to the environment.[1–3] Compared with normal cells, the complex microenvironment of tumor cells makes their mitochondria tend to maintain higher redox homeostasis, such as the balance between a higher level of reactive oxygen species (ROS) and the antioxidant GSH, which makes its mitochondrial homeostasis more easily broken.[4–6] For the time being, mitochondrial homeostasis has become a potential research target to kill cancer cells.[7–9] The consumption of GSH in mitochondria or the increase of the ROS level will destroy its redox homeostasis, leading to the rapid accumulation of ROS, which will damage intracellular DNA, proteins and lipids, and then cause cancer cell apoptosis.[10–12] Therefore, the development of a strategy to break this redox homeostasis by rapidly causing the accumulation of ROS in mitochondria is of great significance for cancer treatment.

Photodynamic therapy (PDT), with the advantages of good temporal and spatial control, less systemic side effects and noninvasiveness, has become a promising method for clinical cancer treatment.[13–15] It is mainly composed of three elements: photosensitizer, oxygen and light. Upon delivering the photosensitizer to the target site, the photosensitizer reacts with oxygen molecules under light stimulation to generate highly cytotoxic ROS to damage or kill the target cells.[16,17] Although PDT has made some progress in the treatment of cancer, its sustained killing effect on tumor cells is not satisfactory due to low production of ROS and short lifetime, poor tissue penetration depth of light, hypoxia of the tumor microenvironment and other problems.[18–20] In order to improve its therapeutic effect, in recent years, the development of organelle-targeted PDT has become a popular choice, especially for mitochondria.[21–24] However, due to the high redox homeosta-

[a]*Fujian Provincial Key Laboratory of Innovative Drug Target Research and State Key Laboratory of Cellular Stress Biology, School of Pharmaceutical Sciences, Xiamen University, Xiamen, 361102, China. E-mail: wuyl@xmu.edu.cn*
[b]*Department of Materials Science and Engineering, National University of Singapore, 9 Engineering Drive 1, 117576 Singapore. E-mail: lizb@imre.a-star.edu.sg, msehc@nus.edu.sg*
[c]*Institute of Materials Research and Engineering, A*STAR (Agency for Science, Technology and Research), 2 Fusionopolis Way, Innovis, #08-03, 138634 Singapore*
†Electronic supplementary information (ESI) available. See DOI: 10.1039/d1nr06214j
‡Both authors contributed equally to this work.

sis of intracellular mitochondria (*e.g.*, high GSH content), targeting mitochondria alone can improve its anti-tumor effect to a certain extent, but the reactive oxygen species produced by PDT cannot continue to kill cancer cells, especially the deep hypoxic microenvironment of solid tumors. Therefore, there is an urgent need for a strategy to increase the ROS production of PDT and solve the hypoxia problem in the deep part of the tumor tissue to continuously and effectively kill tumor cells.

Enzymes, as a kind of biocatalyst with high catalytic efficiency and strong substrate affinity, have been widely used in the research of disease diagnosis and tumor treatment.[25–28] Recently, researchers have found that nanomaterials, including enzymes or enzyme-like nanomaterials, have the potential to enhance the effectiveness of photodynamic therapy.[29–32] For example, Peng's team encapsulated catalase and the photosensitizer into liposomes, and used catalase to catalyze the high level of H_2O_2 in tumors to produce O_2 to enhance the efficacy of photodynamic therapy.[33] Xing *et al.* constructed an Au_2Pt nanozyme with catalase and peroxidase-like activity, which can simultaneously produce oxygen and $^{\bullet}OH$, thereby synergizing photodynamic and chemodynamic therapy to kill cancer cells.[34] Nevertheless, the endogenous H_2O_2 concentration of tumor cells is limited, which is not enough to achieve satisfactory catalytic treatment efficiency. The enzyme cascade catalytic reaction provides new ideas for further improving the curative effect of photodynamics.[35] Wu *et al.* designed a P@Pt@P-Au-FA nanoreactor with GOX and CAT activity, which uses Pt NPs to catalyze H_2O_2 in tumor cells to produce O_2, and further accelerate Au NPs to catalyze glucose in tumor cells to produce H_2O_2, so as to achieve cyclic catalytic amplification.[36] However, most of these nanoreactors are composed of metals or metal oxides, and their catalytic efficiency, biosecurity and histocompatibility are still of concern.[37–40] In contrast, natural enzymes not only have high catalytic efficiency and strong substrate affinity, but also have good biocompatibility and safety. Zhang *et al.* constructed a bioreactor by loading GOX and CAT into a metal–organic framework PCN-224 and coating it with cancer cells to achieve the endogenous circulating supply of O_2 and H_2O_2, which greatly improved the photodynamic efficacy.[41] However, the current construction of such a bioreactor catalyst is too cumbersome, and the ratio of enzymes and the space distance between each other still need to be considered in the design to develop a simpler, safer, and more efficient bioreactor structure.

Here, we construct a high-efficiency mitochondrial targeted bioreactor containing GOX, CAT and PpIX through a simple preparation method (Scheme 1). Under the action of the mitochondrial target head TPP, the bioreactor can accurately locate the mitochondria of breast cancer 4T1 cells to achieve a safe and efficient sequential catalytic reaction through the reasonable ratio and spatial distance of the two enzymes. It can use GOX to consume glucose, the energy source of tumors, to produce H_2O_2, and CAT, which is close to GOX in space, can quickly catalyze cytotoxic H_2O_2 to produce O_2 to prevent damage to normal cells. The bioreactor uses GOX to consume glucose in cancer cells to produce H_2O_2; meanwhile, CAT located close to GOX quickly catalyzes cytotoxic H_2O_2 to produce O_2, preventing damage to normal cells. The generated O_2 further accelerates GOX to continue to catalyze glucose while being used as the photosensitizer PpIX to produce ROS, which achieves efficient circulatory glucose consumption and cell mitochondrial damage, thereby effectively synergizing starvation therapy and PDT, and improving cancer treatment effects. This simple, safe and efficient mitochondrial targeted

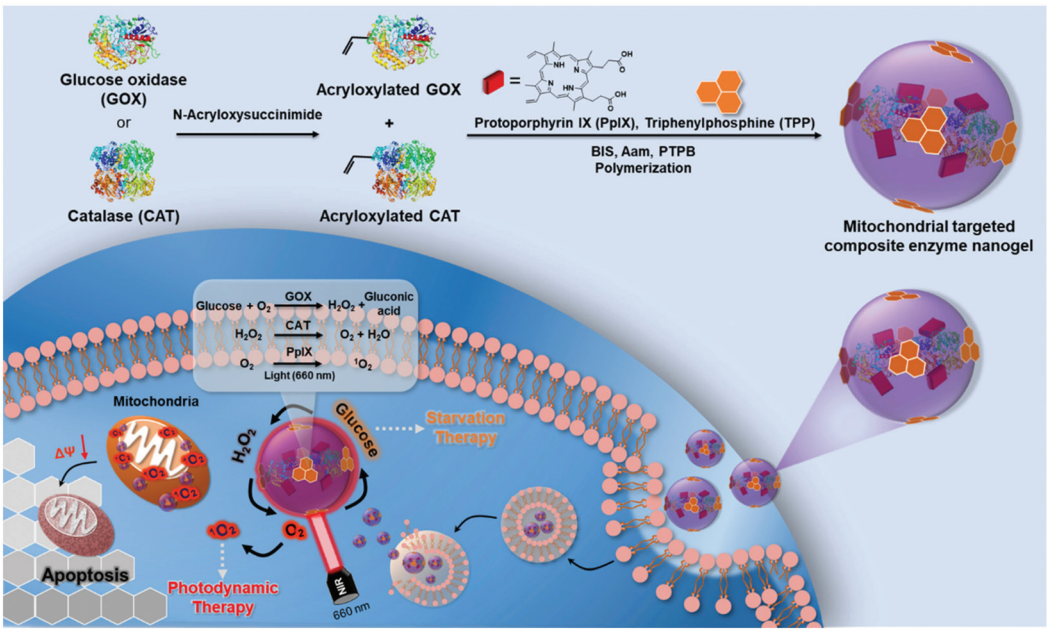

Scheme 1 The design of composite enzyme nanogels for synergistic starvation and photodynamic therapy.

cycle biocatalytic reactor provides a promising new strategy for cancer treatment.

The mitochondria targeted GOX-CAT-PpIX (tGCP) nanogel was prepared by making polymerization using acryloxylated GOX and acryloxylated CAT together with protoporphyrin IX (PpIX), acrylamide (AAm), *N*,*N*′-methylene bisacrylamide (BIS) and mitochondria targeted monomers (TPP). Transmission electron microscopy (TEM) was employed to observe the fabricated nanogels, as shown in Fig. 1A, and a spherical architecture with a size of around 65 nm was observed, confirming the formation of nanogels. The dynamic light scattering (DLS) image suggested that the nanogel was formed with a size of 68 nm, which was larger than the size of CAT (8.7 nm) and GOX (6.5 nm) (Fig. S1†). The UV-Vis spectrum of the nanogel showed the absorption of porphyrin, providing the possibility of photodynamic therapy using this nanogel (Fig. 1B). We then modified FITC and Rhodamine B (RhB) onto GOX and CAT, respectively, and prepared the nanogel using the same approach to obtain a fluorescence-labeled GOX-CAT (FGC) nanogel. As shown in Fig. 1C, when excited at 450 nm, the mixture of FITC-GOX and RhB-CAT mainly showed the emission fluorescence spectrum of FITC from 480 nm to 650 nm, however, the emission intensity of FITC decreased and the emission spectrum of RhB centered at 580 nm emerged, implying that a fluorescence resonance energy transfer (FRET) phenomenon occurred from FITC-GOX to RhB-CAT within this nanogel, showing close spatial proximity between the GOX and CAT of the enzyme nanogel.[42]

Since glucose can be oxidized to gluconic acid and H_2O_2 by GOX in the presence of oxygen, the pH value and the oxygen content of the solution should be decreased. As shown in Fig. 1D, when glucose was added into the tGCP nanogel solution, the nanogel solution pH value decreased gradually from 6.5 to 3.7 within 615 min because of the generation of gluconic acid, similar to that of GOX solution. Nevertheless, the pH value of the glucose aqueous solution remained almost unchanged. Meanwhile, the oxygen level in mitochondria targeted GOX-PpIX (tGP) nanogel solution decreased sharply from 4.86 mg L^{-1} to 0 within 240 s, however, the oxygen level in the tGCP nanogel decreased more slowly, which can be attributed to the breakdown of hydrogen peroxide catalyzed by CAT in the tGCP nanogel to generate oxygen. When the tGCP nanogel was incubated with H_2O_2, oxygen bubbles generated by CAT catalyzed H_2O_2 decomposition can be observed in the macroscopic images (Fig. S2†). Because CAT in the tGCP nanogel would influence the estimation of GOX activity in the tGCP nanogel, we used the GOX-PpIX nanogel, whose preparation process was the same as that of the tGCP nanogel, but PTPB and CAT were removed, as a substitution to assess the effect of polymerization on GOX activity. Fig. S3† shows that GOX and CAT respectively retained 89.3% and 96.9% of their original activity after the polymerization reaction. Furthermore, in comparison with the mixture of native GOX and CAT, the stability of the cascade catalytic activity between GOX and CAT within the tGCP nanogel was significantly improved (Fig. S4†).

The cascade generation of $^1O_2$ induced by PpIX in the tGCP nanogel following glucose decomposition and oxygen generation was estimated by using singlet oxygen sensor green (SOSG) as the indicator, whose fluorescence intensity would

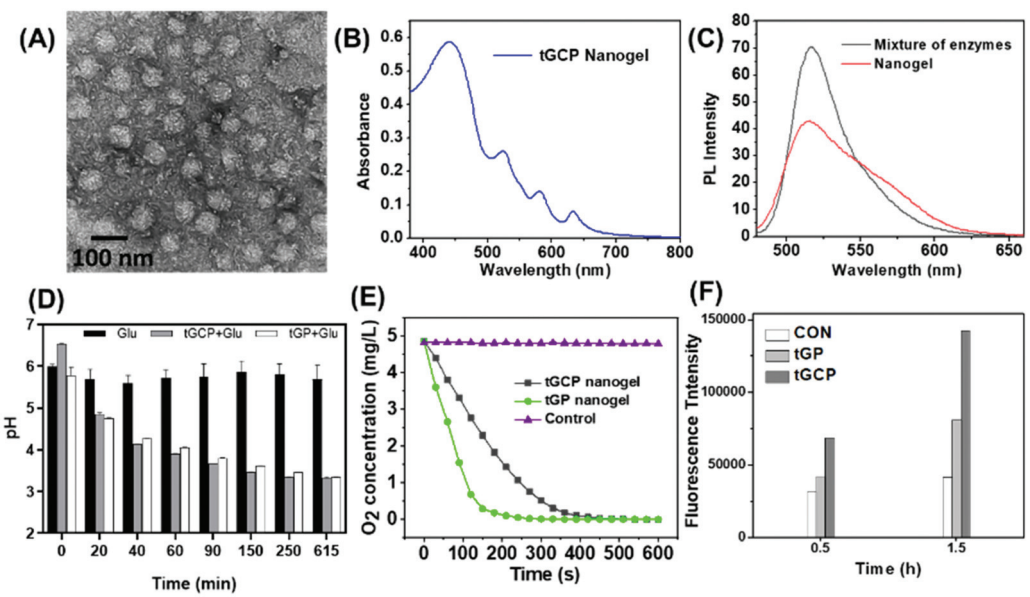

Fig. 1 (A) TEM image of the fabricated tGCP nanogel (nanogel was stained with phosphotungstic acid). (B) UV-Vis spectrum of the tGCP nanogel in PBS. (C) Fluorescence spectra of the nanogel fabricated from FITC-GOX and RhB-CAT, and the mixture of FITC-GOX and RhB-CAT upon excitation at 450 nm. (D) pH changes of the tGCP and tGP nanogel solution in the presence of glucose. (E) Oxygen content changes of the aqueous solution of the tGCP and tGP nanogels in the presence of glucose. (F) Fluorescence changes of the SOSG treated with the tGCP and tGP nanogels in the presence of light and glucose (1 mg mL^{-1}).

increase in the presence of $^1O_2$. As shown in Fig. 1F, when SOSG was treated with tGP or tGCP together with light in the presence of glucose, the intensity of SOSG greatly increased within 1.5 h in comparison with the control sample, indicating the generation of $^1O_2$. The results above successfully demonstrated the cascade reactions between GOX, CAT, and PpIX in the tGCP nanogel. Because of the oxygen dependent glucose oxidation reaction and $^1O_2$ production, the designed tGCP nanogel with oxygen self-production ability presented great potential in killing the tumor tissue by improving PDT and starvation therapy.

In order to evaluate the ability of the composite enzyme nanogel to kill tumor cells *in vitro*, we selected 4T1 cells as model cells, as shown in Fig. 2. From Fig. 2A, it can be seen that under laser irradiation conditions, the tGCP-light group showed a stronger killing effect on 4T1 cells compared with the non-illuminated composite enzyme group (tGCP). This may be because GOX in the composite enzyme can consume glucose in the medium to produce H_2O_2, and H_2O_2 is further catalyzed by CAT to produce O_2, thereby enhancing the therapeutic effect of PDT. In addition, compared with the GCP-light group, tGCP-light with a mitochondrial target showed a better cancer cell killing effect. It is worth noting that the tGP group showed the strongest 4T1 cytotoxicity, which may be due to the high toxicity of the strong oxidative H_2O_2 produced by GOX catalyzed by glucose. As can be seen from the Fig. S5D,† H_2O_2 has obvious toxicity to 4T1 cells when the concentration reaches 200 μg mL^{-1}. In the tGCP group without light, due to the close spatial position of CAT and GOX, it can quickly catalyze H_2O_2 to produce O_2, so it is safer for cells. In order to further prove the safety of the composite enzyme, we selected LO2 cells for further evaluation. It can be seen from Fig. 2B and C that in either high-sugar or low-sugar medium, the GOX group (tGP) alone showed obvious LO2 cytotoxicity. In the low-sugar RPMI medium, tGCP shows low toxicity to LO2 cells, which indicates that the nanocomposite enzyme has good safety to normal cells, and lays the foundation for its application and promotion. Due to certain errors in MTT analysis, we further performed cytotoxicity analysis by flow cytometry, as shown in Fig. S5.† The results of flow cytometry are basically the same as those of MTT. It is worth noting that from Fig. S5A and S5B,† under light conditions, the tGCP group with mitochondrial targets has a stronger killing effect on cancer cells than the GCP group, and it also has a better antitumor effect than tGP alone with an increase in the concentration. In addition, it can be seen from Fig. S5C† that the tGCP group still showed low toxicity to normal cells, LO2 cells. In order to verify the blood compatibility of the compound enzyme, we also performed a hemolysis test on the composite enzyme nanogel, as shown in Fig. 2D. It can be seen that the

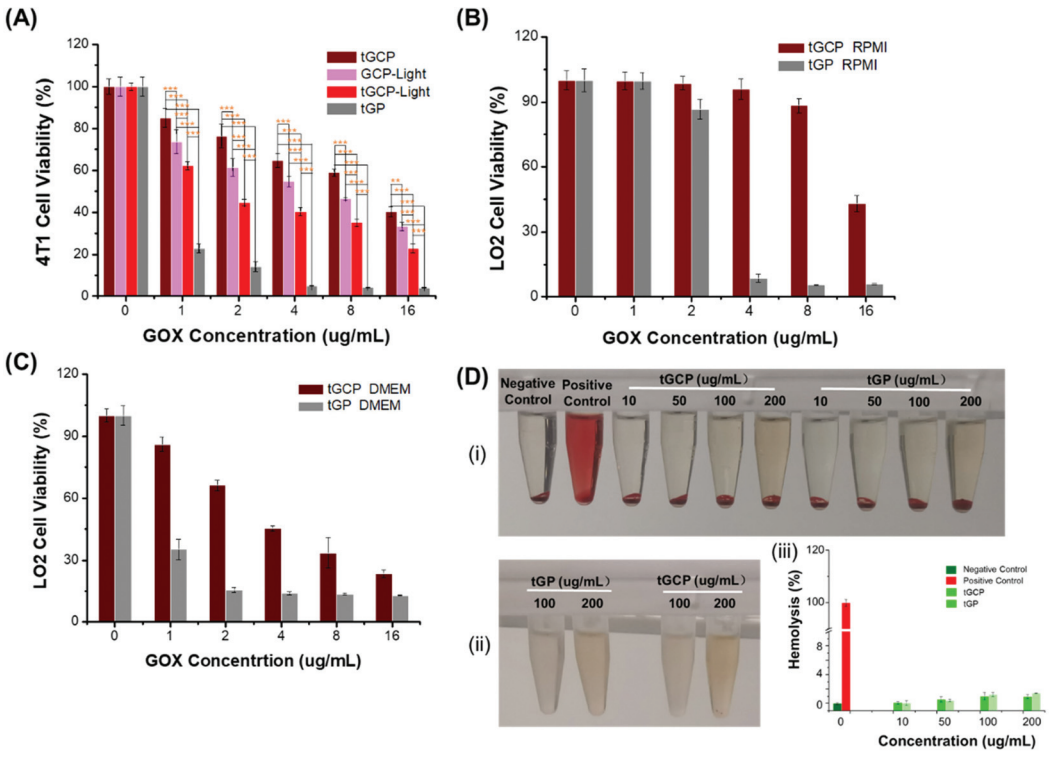

Fig. 2 Cell viability of 4T1 cells and LO2 cells treated with different nanogels. (A) Cell viability of 4T1 cells treated with tGCP, GCP, and tGCP with a laser (660 nm, 100 mW cm^{-2}) and tGP in DMEM, respectively. (The statistical significance was obtained through two-way ANOVA and Bonferroni's post-hoc tests using GraphPad 5.0, n = 5, $^{**}P < 0.01$, $^{***}P < 0.001$.) Cell viability of LO2 cells treated with tGCP and tGP in (B) RPMI medium (without glucose) and (C) DMEM (with glucose). (D) (i) Hemolysis images of different composite enzyme nanoparticles, (ii) images of different concentrations of composite enzyme nanogels (without red blood cells) as hemolysis controls, (iii) quantitative column chart of hemolysis analysis.

nanogel has good blood compatibility, even at a concentration of up to 200 μg mL^{-1}, and the hemolysis rate is only about 1% (Fig. 2D(iii)), and neither of them shows an obvious hemolysis phenomenon. Noticeably, the supernatant appears slightly red at a concentration of 200 μg mL^{-1} in Fig. 2D(i), compared with Fig. 2D(ii), which can be found to be the result of the color of the material itself.

As an important source of energy for cells, mitochondria will release apoptosis-inducing factors and trigger cell apoptosis when they are damaged by stimuli such as reactive oxygen species. Only by effectively delivering the generated ROS composite enzyme nanogel to the mitochondria, its anti-tumor effect can be better played. In order to verify the mitochondrial targeting effect of the composite enzyme nanogel, we observed the mitochondrial co-location effect of different nanoadhesive using a confocal microscope, as shown in Fig. 3. As can be seen from Fig. 3A and B, with or without mitochondrial TPP target, the cell's intake of composite enzymes gradually increases over time. Compared with the GCP group without a TPP target, 4T1 cells had significantly more uptake of the composite enzyme nanogel with a mitochondrial TPP target (tGCP), showing stronger green fluorescence, and more overlap between green fluorescence and red fluorescence could be seen, indicating that it had a very good mitochondrial co-localization effect. In order to display this co-localization effect more intuitionally, we further analyzed the coincidence effect of green fluorescence and red fluorescence in cells at 12 h using the Image J software, as shown in Fig. 3C and D. As can be seen from the figure, compared with the GCP group without a mitochondrial target, the red and green lines in the tGCP group tended to be more synchronous, indicating that the mitochondrial targeting of the nanogel could be effectively increased after the TPP target modification.

To further verify the photodynamic therapeutic effect of the compound enzyme nanogel, we used DCFH-DA to detect the ROS production in 4T1 cells, as shown in Fig. 4A. As can be seen from Fig. 4A, the tGCP group under light conditions could observe the strongest green fluorescence, indicating that the composite enzyme nanogel could effectively generate cytotoxic ROS, which caused significant changes in cell morphology as shown in the bright field diagram. It should be noted that, compared with the blank control group, the morphology of clear field cells in the tGCP group was not significantly different from that in the control group, but a certain amount of green fluorescence could also be observed in the tGCP group with light. This may be due to the fact that H_2O_2 produced by GOX catalyzed glucose was not consumed by CAT in time, and there was also a strong reaction with DCFH-DA. However, according to the bright field diagram, these ROS did not produce obvious toxicity to cells, which indicated the safety of the composite enzyme nanogel. It is noteworthy that the tGP group can also observe strong green fluorescence, which is the result of GOX catalyzed glucose generation of H_2O_2, which is also the reason why it shows strong cytotoxicity in MTT. In addition, since the number of cells in each figure was not consistent, we used the Image J software to analyze

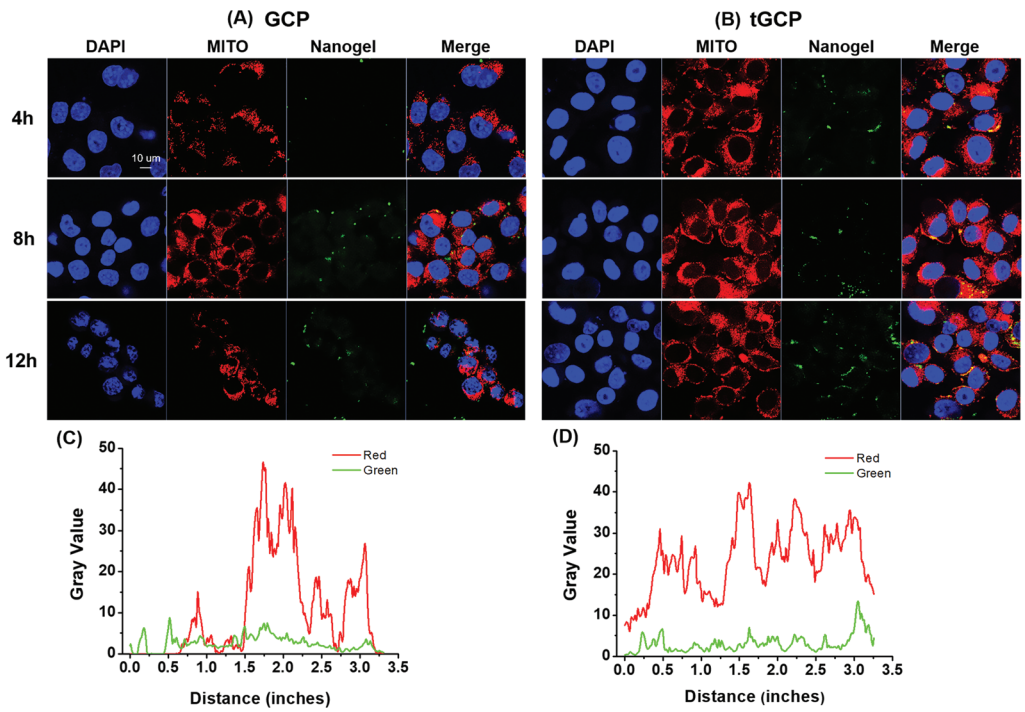

Fig. 3 Confocal images of mitochondria targeting in 4T1 cells treated with (A) GCP (without TPP) and (B) tGCP (with TPP) at different times. Mitochondrial colocalization analysis diagram (red represents mitochondria, green represents nanogels) of 4T1 cells treated with (C) GCP and (D) tGCP at 12 h.

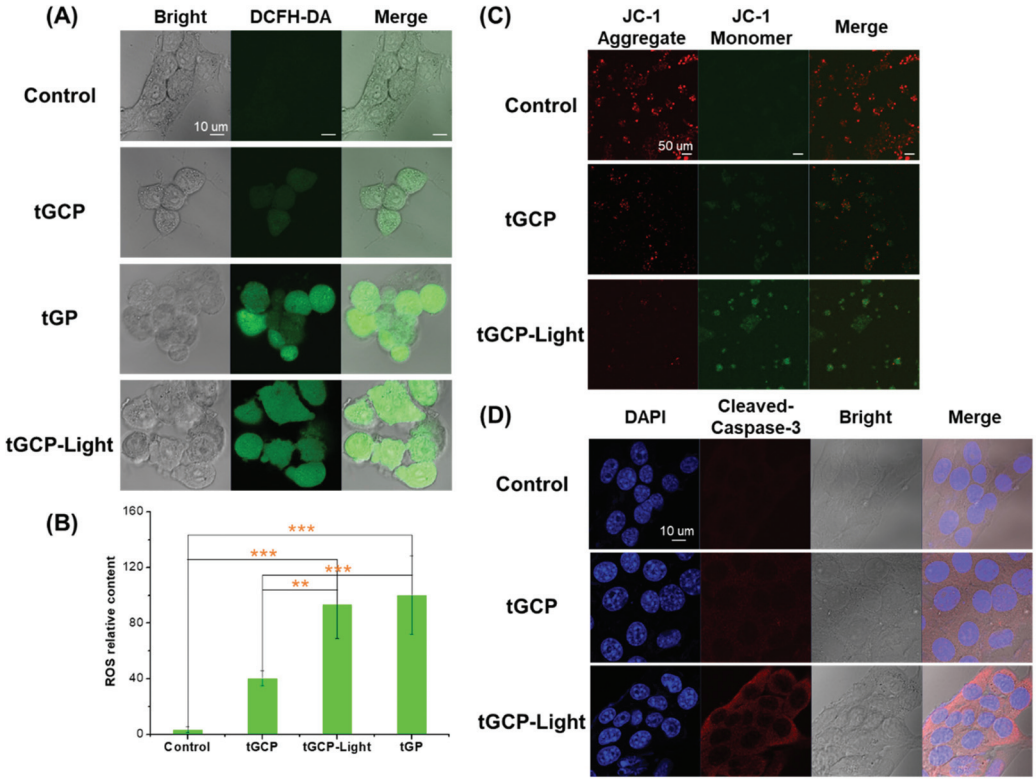

Fig. 4 (A) Fluorescence images of ROS generation in 4T1 cells treated with tGCP. (B) Relative ROS fluorescence intensity average value in 4T1 cells after treatment under different conditions (the statistical significance was obtained through one-way ANOVA and Tukey's post-hoc tests by using GraphPad 5.0, $^{**}P < 0.01$, $^{***}P < 0.001$). (C) Confocal fluorescence images of mitochondrial membrane potential analysis obtained by JC-1 measurement in 4T1 cells treated with different treatment methods. (D) The analysis of caspase-3 activity in 4T1 cells treated with different treatment methods.

the relative average fluorescence intensity of the cells, as shown in Fig. 4B. It can also be seen that the average ROS content in the tGCP-light group under the light conditions showed the most, indicating that light can effectively increase the ROS production of the composite enzyme nanogel to improve the effect of PDT. The change in the mitochondrial membrane potential is an important sign of early apoptosis of cells. In order to study the mitochondria-specific damage ability of the composite enzyme nanogel, a JC-1 kit was used to detect the cell mitochondrial membrane potential, as shown in Fig. 4C. Due to the higher mitochondrial membrane potential in healthy cells, JC-1 dye tended to form aggregates and presented red fluorescence, while in unhealthy or apoptotic cells, the mitochondrial membrane potential was lower, and the JC-1 dye presented green fluorescence as a monomer. As can be seen from Fig. 4C, compared with the other groups, the tGCP group under light had significantly more green fluorescence and less red fluorescence, indicating that the cell mitochondrial membrane potential was low at this time, reflecting the poor state or apoptosis of the cell at this time. These results indicate that the composite enzyme nanogel can produce ROS under light conditions, which can effectively damage the mitochondria of cancer cells and cause cell apoptosis. Cytochrome c and caspase-3 are important marker proteins of the mitochondrial apoptosis pathway, so we supplemented the immunofluorescence experiment for the release of cytochrome c from mitochondria and caspase-3 activation, as shown in Fig. 4D and Fig. S6.† As can be seen from these figures, cytochrome C was significantly released from mitochondria and caspase-3 activation can be clearly seen in 4T1 cells treated with mitochondria-targeted composite enzyme nanogels (tGCP-light) under light (660 nm, 100 mW cm^{-2}). Combined with the change in the mitochondrial membrane potential, it can be inferred that the cell apoptosis caused by the composite enzyme nanogels is mainly through the mitochondrial apoptosis pathway.

Next, we established a 4T1 breast cancer mouse model to investigate the *in vivo* antitumor effect of the composite enzyme nanogel, as shown in Fig. 5. According to Fig. 5A and B, the GCP-light group, tGP-light group and tGCP-light group all showed anti-tumor effects under light conditions, among which the tGCP-light group showed the best anti-tumor effect with a tumor volume of about 45 mm^3, followed by the tGP-light and GCP-light group with tumor volumes of about 119 mm^3 and 268 mm^3, respectively. This may be because GOX consumes the tumor energy source glucose to generate H_2O_2, which can be effectively catalyzed by CAT to generate O_2 to enhance PDT, and thus effectively inhibiting tumor growth

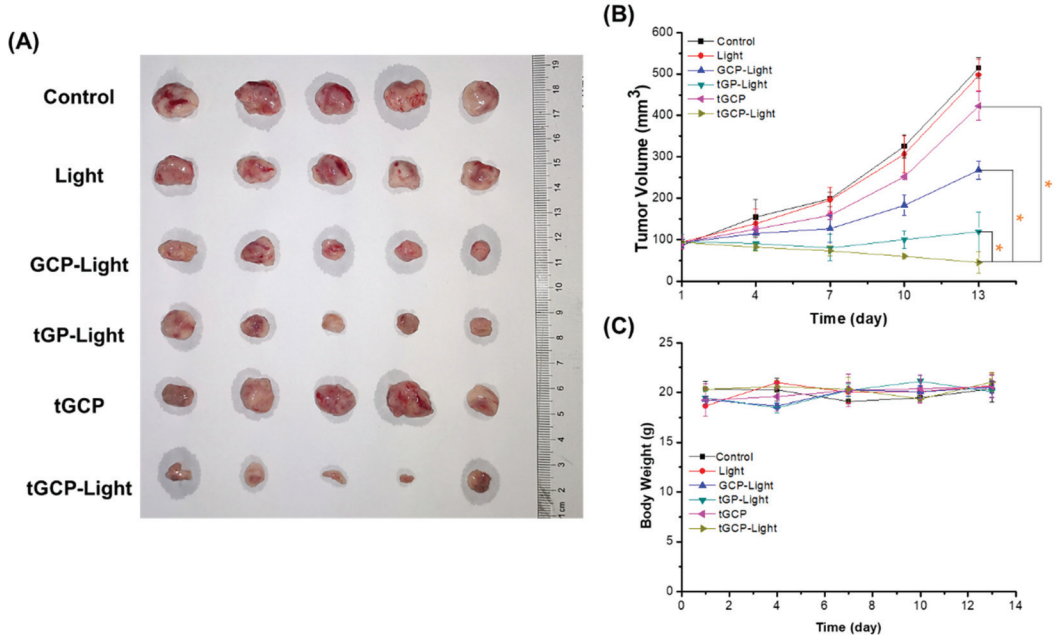

Fig. 5 Anti-tumor effect of composite enzyme nanogels *in vivo*. (A) Pictures of tumors removed from mice in different treatment groups. (B) Curve of the tumor volume over time in different treatment groups (the statistical significance was obtained through two-tailed Student's tests using GraphPad 5.0, $n = 5$, $^*P < 0.05$). (C) Curve of the body weights of mice in different treatment groups over time.

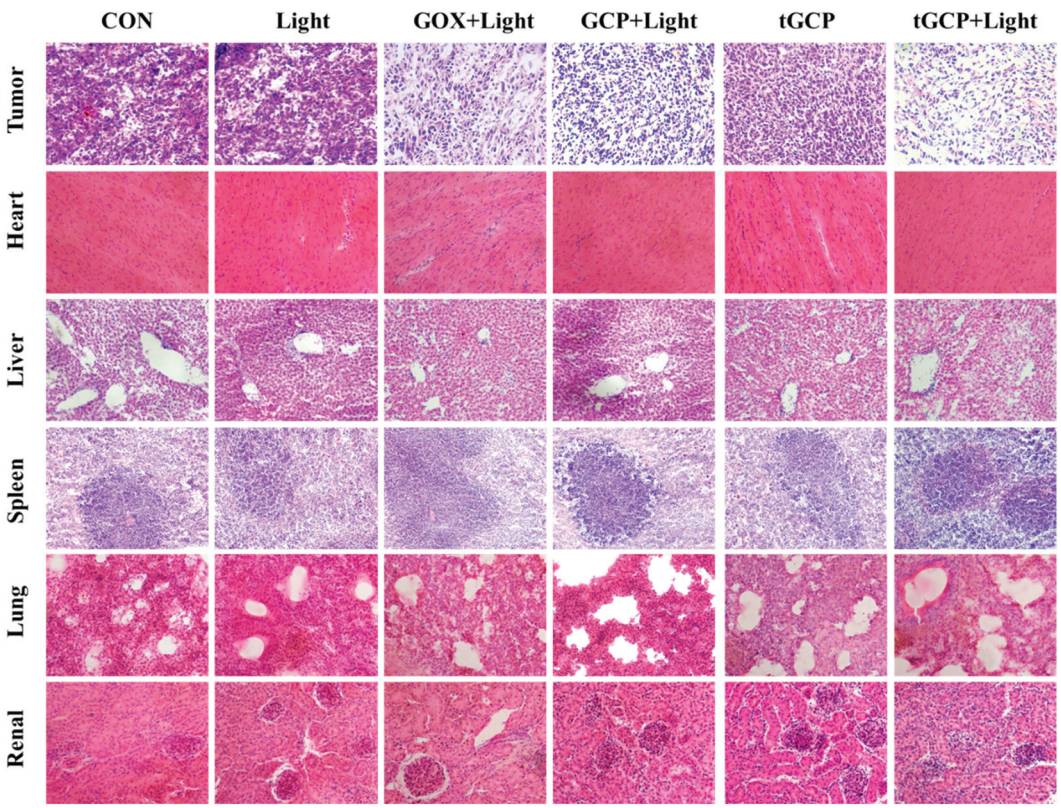

Fig. 6 H&E staining images of the tumors and main organs of mice.

through synergistic starvation and PDT. It is worth noting that the tGP group showed better 4T1 cell inhibition in cell experiments than the tGCP-light group, but in animal experiments, it did not perform better. This may be due to the more complex tumor microenvironment, such as a variety of enzymes, and part of the highly toxic H_2O_2 catalyzed by GOX

may be depleted. In addition, the tGP-light group has a better tumor suppressor effect than the GCP-light group, which may be because tGP can effectively target cell mitochondria, and can effectively damage mitochondria through the generation of highly cytotoxic H_2O_2 combined with ROS generated by PDT. Interestingly, it can be seen from Fig. 5B that tGP-light and GCP-light groups showed significant inhibitory effects in the early stage, and the inhibitory effect was significantly weakened in the later stage, which may be attributed to tumor hypoxia in the later stage and effective energy supply by tumor neovascularization. Moreover, we measured the body weight of the mice to evaluate the safety of these nanogels. As shown in Fig. 5C, the different nanogel preparation groups did not show significant weight changes, indicating that these composite enzyme nanogels are safe and reliable.

The antitumor effect and biosafety of composite enzyme nanogels were investigated by histological analysis of tumors and major organs in H&E staining. Purple represents the nucleus and red represents the cytoplasm, as shown in Fig. 6. As can be seen from the figure, the tumor tissue in the GCP-light, tGP-light, and tGCP-light groups under light conditions was significantly less purple than in the other groups. Among them, the tGCP-light group showed the least purple, and the tissue in the section showed more post-apoptotic spaces, indicating that synergistic starvation and self-oxygenated PDT had an excellent antitumor effect. Tumor sections showed results consistent with tumor suppressive experiments in animals. In addition, there was no significant difference in the sections of the main organs of different nanogels, indicating that the composite enzyme nanogels did not cause significant damage to the organs of mice, which fully demonstrated its excellent biocompatibility and biosafety.

Conclusions

In summary, we have prepared a mitochondrial targeting composite enzyme nanogel with a circulating self-supply of O_2 and H_2O_2 through a simple synthesis method. By a reasonable ratio and spatial position of GOX and CAT, sequential cascade catalysis of the composite enzyme can be realized to continuously consume glucose and realize the cyclic production of H_2O_2 and O_2. The nanogel can well target the mitochondria of tumor cells, enhance the PDT generation of ROS through cyclic catalysis to destroy the mitochondria of cancer cells, thus resulting in cell apoptosis. At the same time, it is relatively safe for normal cells, because the cascade of composite enzymes consumes highly toxic H_2O_2. In addition, in animal experiments, the composite enzyme group showed a good antitumor effect under light conditions. This is because the composite enzymes continue to consume the tumor energy source glucose to produce enough oxygen, thereby effectively synergizing starvation therapy and photodynamic therapy. The safety, stability, biocompatibility and cascade catalytic efficiency of the composite enzyme nanogel system open a new way for the development of safe and efficient cancer therapy.

Conflicts of interest

There are no conflicts to declare.

Acknowledgements

We would like to thank the National Natural Science Foundation of China (81773661) and the A*STAR Research grant for the support of this project. All animal procedures were performed in accordance with the Guidelines for Care and Use of Laboratory Animals of Xiamen University and approved by the Animal Ethics Committee of Xiamen University, IACUC: XMULAC20210092.

Notes and references

1 D. C. Wallace, *Nat. Rev. Cancer*, 2012, **12**, 685–698.
2 S. Vyas, E. Zaganjor and M. C. Haigis, *Cell*, 2016, **166**, 555–566.
3 W.-X. Zong, J. D. Rabinowitz and E. White, *Mol. Cell*, 2016, **61**, 667–676.
4 I. Martínez-Reyes and N. S. Chandel, *Cancer Discovery*, 2014, **4**, 1371.
5 S. S. Sabharwal and P. T. Schumacker, *Nat. Rev. Cancer*, 2014, **14**, 709–721.
6 L. Tong, C.-C. Chuang, S. Wu and L. Zuo, *Cancer Lett.*, 2015, **367**, 18–25.
7 S. E. Weinberg and N. S. Chandel, *Nat. Chem. Biol.*, 2015, **11**, 9–15.
8 N. Gong, X. Ma, X. Ye, Q. Zhou, X. Chen, X. Tan, S. Yao, S. Huo, T. Zhang, S. Chen, X. Teng, X. Hu, J. Yu, Y. Gan, H. Jiang, J. Li and X.-J. Liang, *Nat. Nanotechnol.*, 2019, **14**, 379–387.
9 P. P. Praharaj, B. S. Patro and S. K. Bhutia, *Br. J. Pharmacol.*, 2021, 1–21.
10 J. N. Moloney and T. G. Cotter, *Semin. Cell Dev. Biol.*, 2018, **80**, 50–64.
11 V. Nogueira and N. Hay, *Clin. Cancer Res.*, 2013, **19**, 4309.
12 Y. Pu, B. Zhou, H. Xiang, W. Wu, H. Yin, W. Yue, Y. Yin, H. Li, Y. Chen and H. Xu, *Biomaterials*, 2020, **259**, 120329.
13 X. Li, J. F. Lovell, J. Yoon and X. Chen, *Nat. Rev. Clin. Oncol.*, 2020, **17**, 657–674.
14 H. Shi and P. J. Sadler, *Br. J. Cancer*, 2020, **123**, 871–873.
15 A. P. Castano, P. Mroz and M. R. Hamblin, *Nat. Rev. Cancer*, 2006, **6**, 535–545.
16 S. S. Lucky, K. C. Soo and Y. Zhang, *Chem. Rev.*, 2015, **115**, 1990–2042.
17 M. Lan, S. Zhao, W. Liu, C.-S. Lee, W. Zhang and P. Wang, *Adv. Healthcare Mater.*, 2019, **8**, 1900132.
18 X. Li, N. Kwon, T. Guo, Z. Liu and J. Yoon, *Angew. Chem., Int. Ed.*, 2018, **57**, 11522–11531.
19 Z. Zhou, J. Song, L. Nie and X. Chen, *Chem. Soc. Rev.*, 2016, **45**, 6597–6626.

20 Y. Song, Q. Shi, C. Zhu, Y. Luo, Q. Lu, H. Li, R. Ye, D. Du and Y. Lin, *Nanoscale*, 2017, **9**, 15813–15824.
21 D. Zhang, L. Wen, R. Huang, H. Wang, X. Hu and D. Xing, *Biomaterials*, 2018, **153**, 14–26.
22 C. Liu, B. Liu, J. Zhao, Z. Di, D. Chen, Z. Gu, L. Li and Y. Zhao, *Angew. Chem.*, 2020, **59**, 2634–2638.
23 Y. Zhang, Y. Cheng, F. Yang, Z. Yuan, W. Wei, H. Lu, H. Dong and X. Zhang, *Nano Today*, 2020, **34**, 100919.
24 J. Qin, N. Gong, Z. Liao, S. Zhang, P. Timashev, S. Huo and X.-J. Liang, *Nanoscale*, 2021, **13**, 7108–7118.
25 M. E. Glasner, J. A. Gerlt and P. C. Babbitt, *Curr. Opin. Chem. Biol.*, 2006, **10**, 492–497.
26 S. J. Benkovic and S. Hammes-Schiffer, *Science*, 2003, **301**, 1196.
27 X. Mei, T. Hu, H. Wang, R. Liang, W. Bu and M. Wei, *Biomaterials*, 2020, **258**, 120257.
28 L.-H. Fu, C. Qi, J. Lin and P. Huang, *Chem. Soc. Rev.*, 2018, **47**, 6454–6472.
29 Z. Liu, T. Li, F. Han, Y. Wang, Y. Gan, J. Shi, T. Wang, M. L. Akhtar and Y. Li, *Biomater. Sci.*, 2019, **7**, 3683–3692.
30 Y. Zhu, H. Shi, T. Li, J. Yu, Z. Guo, J. Cheng and Y. Liu, *ACS Appl. Mater. Interfaces*, 2020, **12**, 18309–18318.
31 L.-H. Fu, Y. Wan, C. Li, C. Qi, T. He, C. Yang, Y. Zhang, J. Lin and P. Huang, *Adv. Funct. Mater.*, 2021, **31**, 2009848.
32 Y. You, D. Xu, X. Pan and X. Ma, *Appl. Mater. Today*, 2019, **16**, 508–517.
33 C. Shi, M. Li, Z. Zhang, Q. Yao, K. Shao, F. Xu, N. Xu, H. Li, J. Fan, W. Sun, J. Du, S. Long, J. Wang and X. Peng, *Biomaterials*, 2020, **233**, 119755.
34 M. Wang, M. Chang, Q. Chen, D. Wang, C. Li, Z. Hou, J. Lin, D. Jin and B. Xing, *Biomaterials*, 2020, **252**, 120093.
35 X. Cai, L. Jiao, H. Yan, Y. Wu, W. Gu, D. Du, Y. Lin and C. Zhu, *Mater. Today*, 2021, **44**, 211–228.
36 C. Liu, J. Xing, O. U. Akakuru, L. Luo, S. Sun, R. Zou, Z. Yu, Q. Fang and A. Wu, *Nano Lett.*, 2019, **19**, 5674–5682.
37 R. Liu, R. Rallo, S. George, Z. Ji, S. Nair, A. E. Nel and Y. Cohen, *Small*, 2011, **7**, 1118–1126.
38 T. Puzyn, B. Rasulev, A. Gajewicz, X. Hu, T. P. Dasari, A. Michalkova, H.-M. Hwang, A. Toropov, D. Leszczynska and J. Leszczynski, *Nat. Nanotechnol.*, 2011, **6**, 175–178.
39 X. Hu, S. Cook, P. Wang and H.-m. Hwang, *Sci. Total Environ.*, 2009, **407**, 3070–3072.
40 P. Makvandi, C.-y. Wang, E. N. Zare, A. Borzacchiello, L.-n. Niu and F. R. Tay, *Adv. Funct. Mater.*, 2020, **30**, 1910021.
41 S.-Y. Li, H. Cheng, B.-R. Xie, W.-X. Qiu, J.-Y. Zeng, C.-X. Li, S.-S. Wan, L. Zhang, W.-L. Liu and X.-Z. Zhang, *ACS Nano*, 2017, **11**, 7006–7018.
42 P. R. Selvin, *Nat. Struct. Biol.*, 2000, **7**, 730–734.